

Article

A Rolling Real-Time Correction Method for Minute Precipitation Forecast Based on Weather Radars

Jin Ding , Jinbing Gao *, Guoping Zhang *, Fang Zhang *, Jing Yang, Shudong Wang, Bing Xue and Kuoyin Wang

Public Meteorological Service Center, China Meteorological Administration, Beijing 100081, China

* Correspondence: magicgao@foxmail.com (J.G.); zhanggp@cma.gov.cn (G.Z.); zhangfangjx@sina.com (F.Z.)

Abstract: The quantitative precipitation estimation by weather radar plays an important role in observations and forecasts of meteorological processes. The National Minute Quantitative Precipitation Forecast system of China (MQPF), providing location-based refined short-term and imminent precipitation forecasting services, filled the gap in the official minute precipitation service products in China's meteorological field. However, due to the technical limitations of radar itself and the complexity of the atmosphere, the corresponding relationship between radar echoes and surface precipitation is unstable. Based on radar and precipitation data from meteorological stations, a rolling real-time correction method is proposed to improve precipitation prediction accuracy through rolling correction of spatial and temporal structural errors in MQPF products. The results show the following: (1) Although this method may lead to a certain increase in the missing ratio, the significant improvement in the false alarm ratio after rolling correction has a positive guiding effect on short-term public meteorological services. (2) Regarding the time to complete rolling correction, the longest and shortest times appear in April and December, respectively. The mean running time to achieve correction of spatial and temporal error corrections ranges from 3.8 s to 6.4 s and 7.7 s to 11.5 s, respectively, which fully meets the real-time operational requirements of radar business.

Keywords: minute precipitation; operational efficiency; radar echo; rainfall intensity; rolling real-time correction



Citation: Ding, J.; Gao, J.; Zhang, G.; Zhang, F.; Yang, J.; Wang, S.; Xue, B.; Wang, K. A Rolling Real-Time Correction Method for Minute Precipitation Forecast Based on Weather Radars. *Water* **2023**, *15*, 1872. <https://doi.org/10.3390/w15101872>

Academic Editor: Quanjia Wang

Received: 11 April 2023

Revised: 8 May 2023

Accepted: 12 May 2023

Published: 15 May 2023



Copyright: © 2023 by the authors. Licensee MDPI, Basel, Switzerland. This article is an open access article distributed under the terms and conditions of the Creative Commons Attribution (CC BY) license (<https://creativecommons.org/licenses/by/4.0/>).

1. Introduction

Precipitation, as an extremely complex weather phenomenon, although it is a key process in the water cycle and has a significant impact on meteorological and hydrological processes, its uncertainty makes precise precipitation prediction a world challenge. Although remote sensing technology is also an effective method [1–3], quantitative precipitation estimation (QPE) by weather radar is important in hydrometeorological observations and forecasts due to a known direct relationship between radar reflectivity and rain rate [4–7]. The most important radar precipitation forecasting system in the world is the MRMS (Multi Radar Multi Sensor system) of the United States [8]. Ware [9] obtained a more accurate QPE by correcting the local station deviation of MRMS radar QPE. The local station deviation correction method includes three steps: (1) the radar station calculates the hourly radar station deviation, (2) interpolates the deviation to the MRMS grid through the inverse range weighted average scheme, and (3) subtracts the interpolated deviation from the hourly radar QPE field. Through cross-validation, the selection of on-line index x can minimize the interpolation error of radar local differences in specific fields every hour. MRMS divides the U.S. land into multiple subdomains, and performs cross-verification and local site correction of radar QPE on each subdomain. Then, the corrected radar QPE from all subdomains is combined at a given time to generate the final U.S. land QPE product.

In China, the main radar precipitation forecasting operational systems include the Severe Weather Automatic Nowcast System (SWAN) developed by the National Meteorological Center of China and the Rainfall Analysis and Prediction Integrated Data Processing

System (RAPIDS) developed by the Hong Kong Observatory [10]. In addition to RAPIDS and SWAN, there is also a system that provides location-based refined short-term and imminent precipitation forecasting services, the National Minute quantitative precipitation forecast system of China (MQPF, <http://www.weather.com.cn/live/>, accessed on 1 May 2023). The MQPF filled the gap of the official minute precipitation service products in China's meteorological field in 2015. Based on the real-time weather radar data and ground minute precipitation observation data of China, MQPF uses the method combined with optical flow extrapolation and machine learning algorithms to establish the relationship between minute precipitation observation and radar echo by extrapolating the echo every 5 min in the next 2 h. Then, the processing system of MQPF can be quickly established through parallel computing and big data processing technology [11].

The SWAN is based on the new generation weather radar data and adopts advanced meteorological algorithms to form a large number of basic products, such as the combined reflectivity factor, echo top and vertical cumulative liquid water content of the radar itself, radar COTREC wind field (continuity of TREC vectors), and one-hour quantitative precipitation forecast (QPF) [12]. It provides useful basic information for the research and development of short-term heavy precipitation identification technology. The radar precipitation rate estimation of SWAN adopts the method of real-time fitting radar reflectivity–rain intensity (Z–I) empirical formula [13], that is, the RASIM (radar gauge synchronous integration method) combined with real-time synchronous integration of radar and rain gauge, to revise the parameters of Z–I empirical formula in real time. The radar precipitation is estimated by using the dynamic classification Z–I relationship method [14], that is, dividing into different levels depended to the radar echo intensity and according to the previous rain gauge and precipitation data, the optimal Z–I parameters are selected from multiple groups of parameters in real-time for the next precipitation estimation.

RAPIDS uses the dynamic correction Z–I relationship of high-frequency rain gauge data to estimate radar precipitation, and realizes the quantitative precipitation prediction fusion of radar extrapolation, proximity prediction, and numerical prediction. Based on the actual grid precipitation, RAPIDS identifies the errors of the falling area and intensity of the mesoscale model precipitation prediction, and uses the phase correction technology to correct the error of the falling area of the model precipitation prediction. At the same time, precipitation intensity predicted by the model is adjusted according to the actual grid precipitation, and the extrapolated predicted precipitation and the corrected model predicted precipitation are fused through the hyperbolic tangent function [15,16]. Two steps are used in RAPIDS to correct the phase of numerical model precipitation prediction: (1) The fast Fourier transform is used to correct the overall displacement deviation of the rain belt, and then the multiscale variational optical flow method is used to adjust the trend of the rain belt and the small-scale precipitation area, so that the precipitation area predicted by the model is more consistent with the actual situation. The model precipitation intensity is adjusted according to the grid fusion quantitative precipitation estimation. It is assumed that the model quantitative precipitation prediction and grid quantitative precipitation estimation field meet the Weber distribution, and the cumulative distribution function is the same. (2) RAPIDS integrates weight allocation. Fusion weight is the embodiment of the fusion method of extrapolation prediction and numerical model prediction, and it is one of the key points of fusion prediction. RAPIDS realizes the fusion of extrapolation prediction and model prediction by dynamically selecting tangent weight. The weight change of the model forecast is represented by a hyperbolic tangent. The two endpoints of the tangent curve are given according to the precipitation weather type and the weather change experience of the forecaster, and different weights are taken under different circumstances in combination with the temporal and spatial scales of different precipitation systems.

However, due to the technical limitations of radar itself and the complexity of the atmosphere, such as abnormal radar observation data, radar observation blind spots, and radar maintenance upgrades, the corresponding relationship between weather radar echoes and surface precipitation is unstable [17]. In addition, in different precipitation processes,

different periods and regions, the same radar echo distribution may also correspond to different precipitation magnitudes. The above situations will affect the accuracy of high-precision precipitation forecasting, leading to a certain degree of false reports and omissions. Ground weather stations provide accurate rainfall, but their lower distribution density limits their more direct use [18]. The deeper combination of weather radar and weather station observations can maximize the complementary advantages, thus improving the accuracy of precipitation prediction [6,19,20]. Through rolling correction, errors and deviations in minute-level precipitation forecasting can be corrected, thereby improving the accuracy and reliability of quantitative precipitation forecasting. For QPE correction in areas with dense ground precipitation stations, previous scholars mainly carried this out by optimizing interpolation methods [21–23] or using machine learning methods to reduce radar estimation errors from weather stations [24,25], but did not carry it out in identifying convection cell or radar echo types. This study will further expand the research of the above ideas. Based on the spatial and temporal structural errors of MQPF, we proposed a rolling real-time correction technique. Compared with other correction methods that directly optimize the Z–R relationship and simply try multiple interpolation methods in space, the innovation of this technology is that it not only innovates the method of radar echo extraction and recognition based on the amount and type of precipitation, but also introduces the idea of parallel correction in both time and space, making the rolling correction results more optimized.

2. Materials and Methods

2.1. Study Area

As the capital of China, Beijing has a large population density and great demand for meteorological services, especially mountain torrents, geological disasters, and urban waterlogging caused by short-term heavy precipitation, which have a serious impact on the safety of people's lives and property. Affected by the warm temperate monsoon climate, four distinct seasons appear in Beijing. As located in the arid and semiarid climate zone, regional differences of precipitation in Beijing are also obvious [26]. From the time scale, precipitation in Beijing is mainly concentrated in summer (June to August). The study selects Beijing and its surroundings, including Beijing, Tianjin, and Hebei Province, with high density of surface meteorological stations and good weather radar observations, as the study area (Figure 1).

The Beijing weather radar station (Beijing radar, ID: Z9010) was established early and can effectively cover Beijing and its suburbs. Beijing radar base data transmission has good real-time performance and integrity. The deviation between the observation and reception time of Beijing radar data is about 60 s. Therefore, it is reasonable to choose Beijing radar base data for the experiment of the method. Radar base data can be obtained from the website of National Meteorological Data Science Center of China (<http://data.cma.cn>, accessed on 1 May 2023). Observed minute precipitation data are obtained from the website of National Meteorological Data Science Center of China (<http://data.cma.cn>, accessed on 1 May 2023). There are abundant meteorological stations around Beijing, and the measured data with high temporal and spatial resolution have great advantages in product correction. In order to ensure the data quality, the missing points and abnormal mutation points of minute data are detected, and then the abnormal points and missing values are removed and interpolated according to the detection results. The data quality control method is the same as the studies by Ding et al. [27,28].

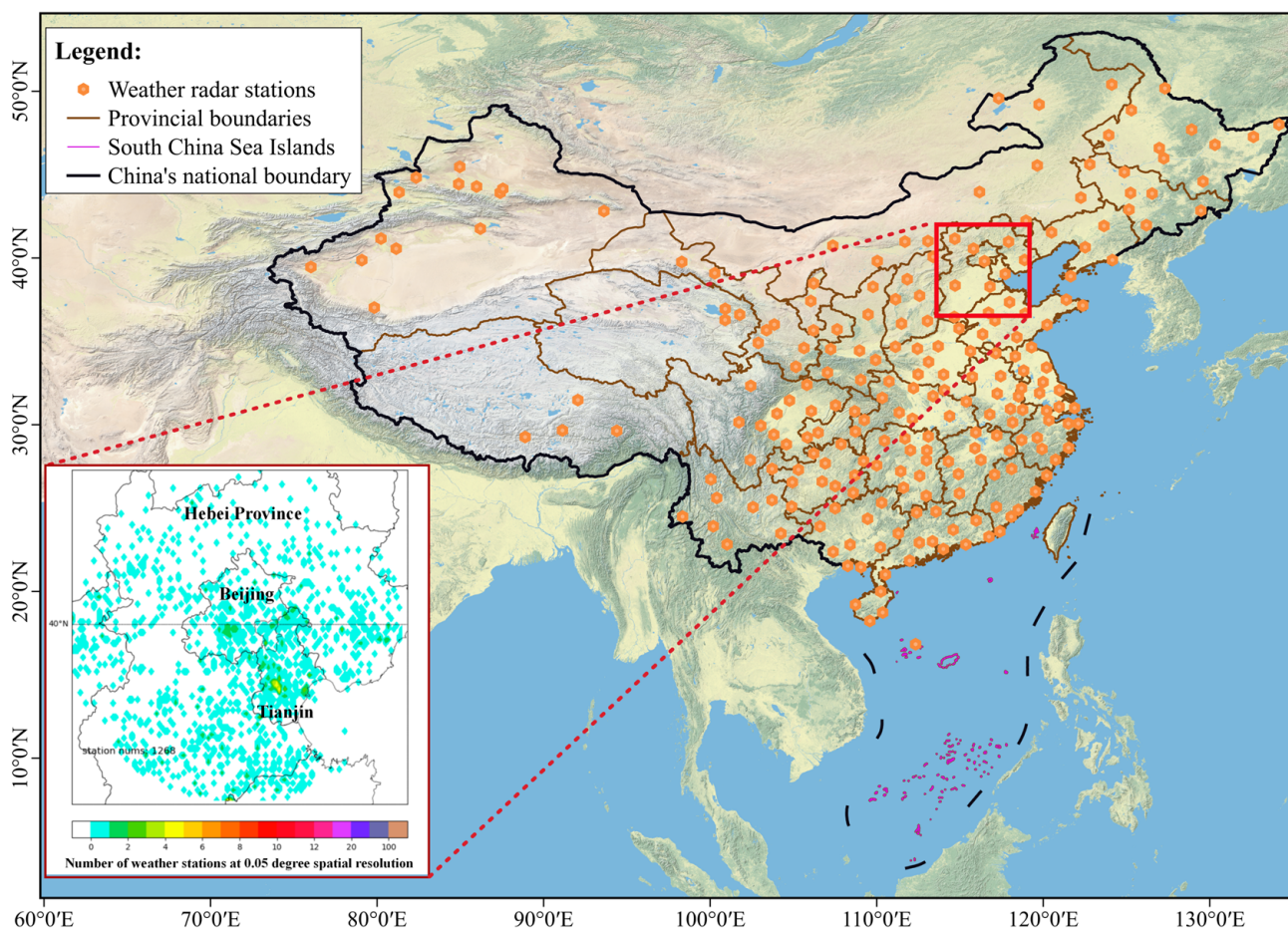


Figure 1. The locations of Beijing and its surroundings and weather radar stations.

2.2. Models

The rolling real-time correction technology proposed in this study relies on the rolling correction of the spatial and temporal structure errors of MQPF products to improve the prediction accuracy, and is verified by a typical precipitation case. For the rolling real-time correction algorithm of spatial structure error of minute precipitation estimation, by distinguishing different echo units in the same radar volume scan, combined with the observed real-time ground precipitation observation data, the regression analysis of precipitation intensity with spatial variation is carried out, and the precipitation prediction correction coefficient of echo units is calculated to correct the spatial structure error of precipitation estimation. For the rolling real-time correction algorithm for time structure error of minute precipitation estimation, by obtaining the observed historical data of ground minute precipitation in the first two hours, the regression analysis of precipitation intensity with time is carried out, and the correction coefficient of precipitation estimation time structure error is calculated to correct the precipitation estimation time structure error. Finally, typical precipitation cases in the study period are selected as the validation dataset to count the quality of minute precipitation products and analyze the results. The technical route is shown in Figure 2.

2.2.1. Radar Echo Monomer Extraction

Radar echo monomer extraction is the basis of rolling real-time update correction according to monomers. Firstly, the precipitation/nonprecipitation echo monomer is identified based on the three-dimensional radar echo characteristics, and then the radar monomer in each time radar volume scan is identified according to the image region segmentation

algorithm (relying on Python programming and its skimage algorithm library) to generate the radar echo monomer data structure for the next error correction.

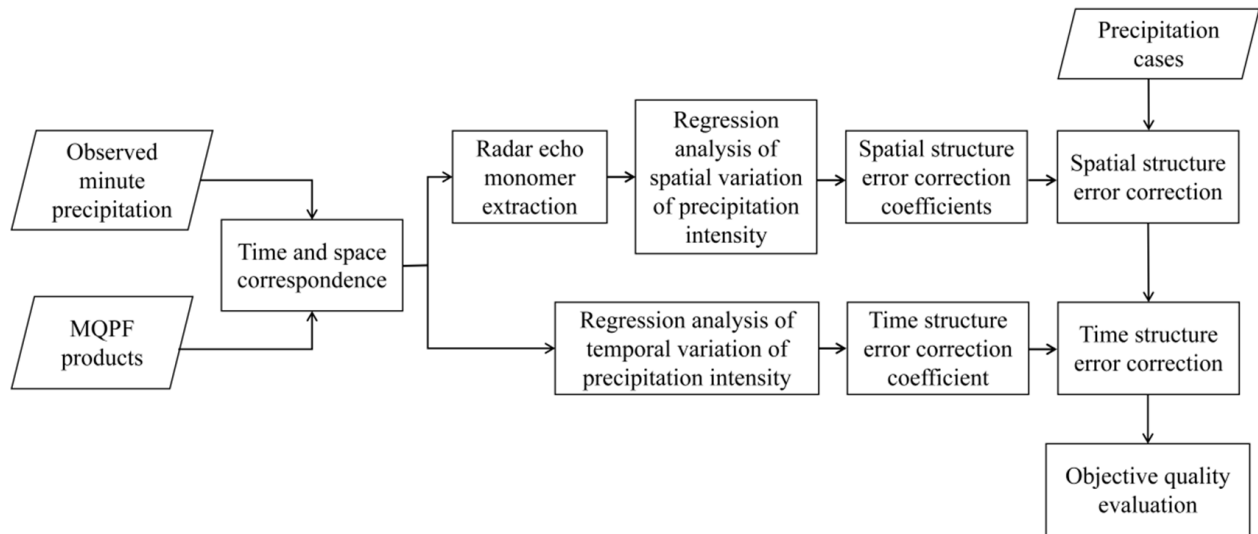
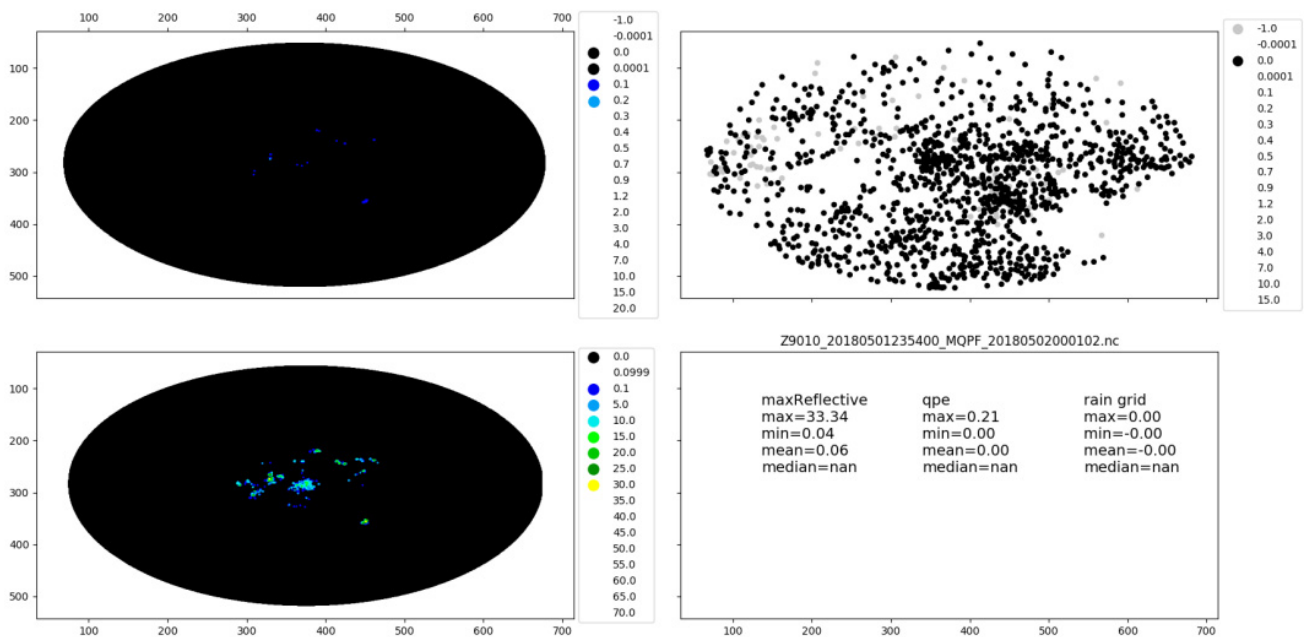


Figure 2. Overall technical roadmap of rolling real-time correction technology.

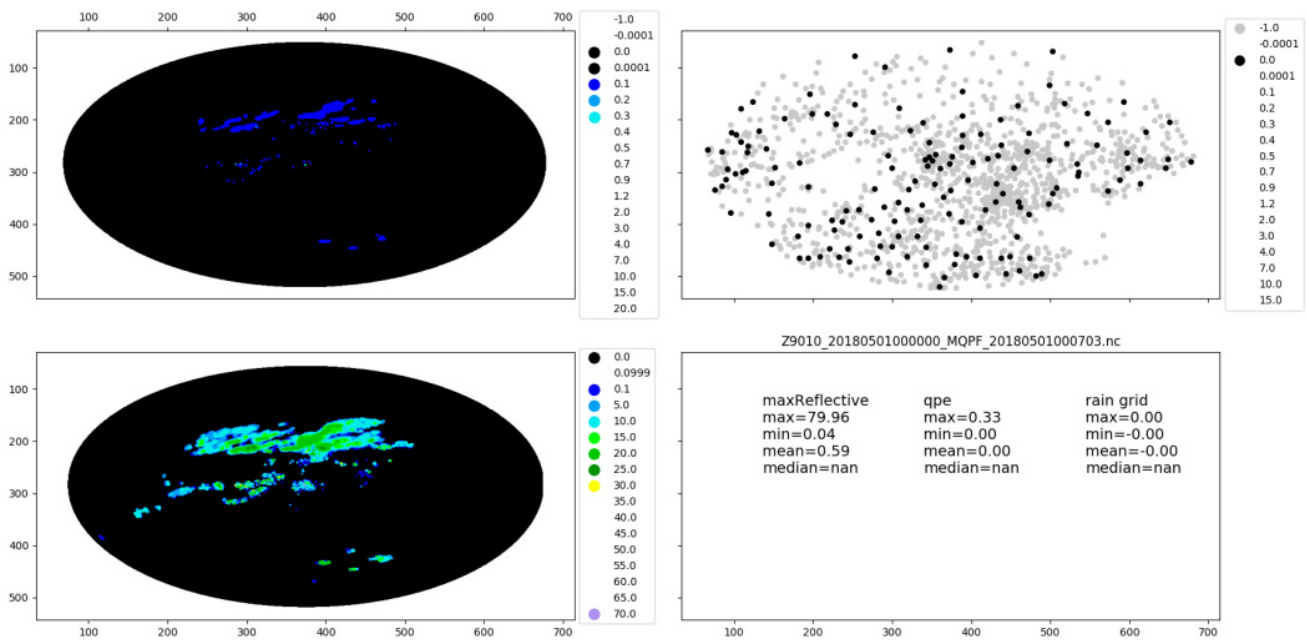
Precipitation/Nonprecipitation Echo Monomer Recognition Technology

Precipitation/nonprecipitation echo monomer recognition is based on three-dimensional radar echo characteristics. According to the characteristics of radar three-dimensional echo, the support vector machine (SVM) [29] is used to train multiple classifiers to classify five types of echo that can cover most echo types, namely, point nonprecipitation echo (Figure 3a), flake nonprecipitation echo (Figure 3b), clear sky nonprecipitation echo (Figure 3c), clear sky mixed flake nonprecipitation echo (Figure 3d), and precipitation echo (Figure 3e).

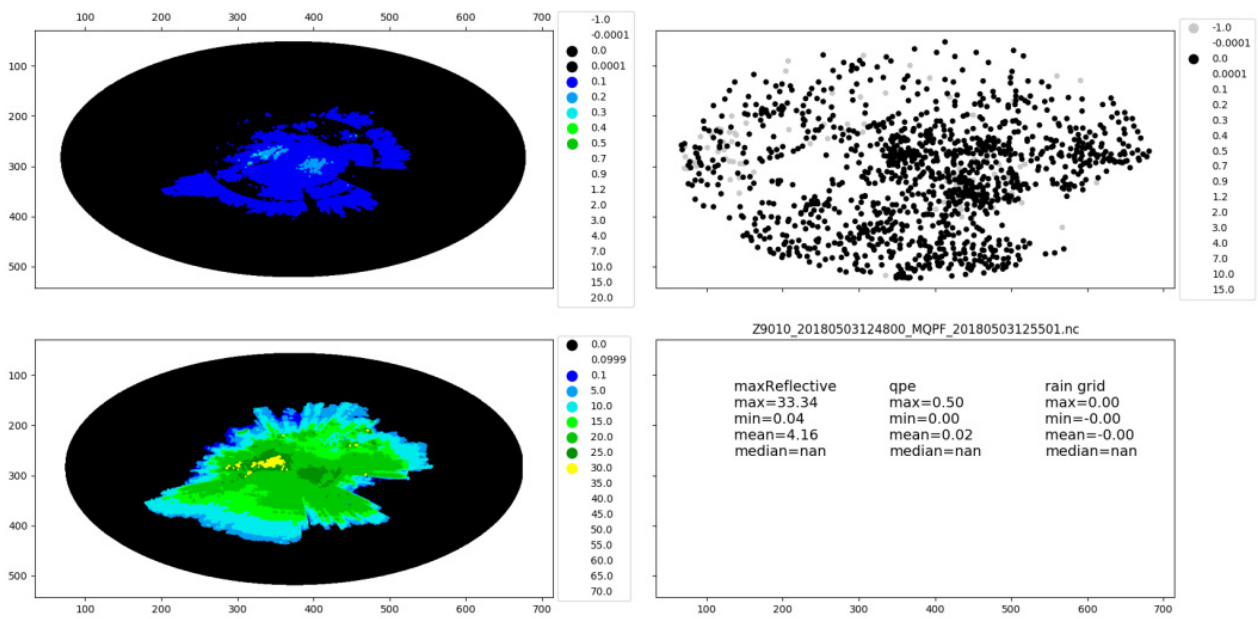


(a)

Figure 3. Cont.



(b)



(c)

Figure 3. Cont.

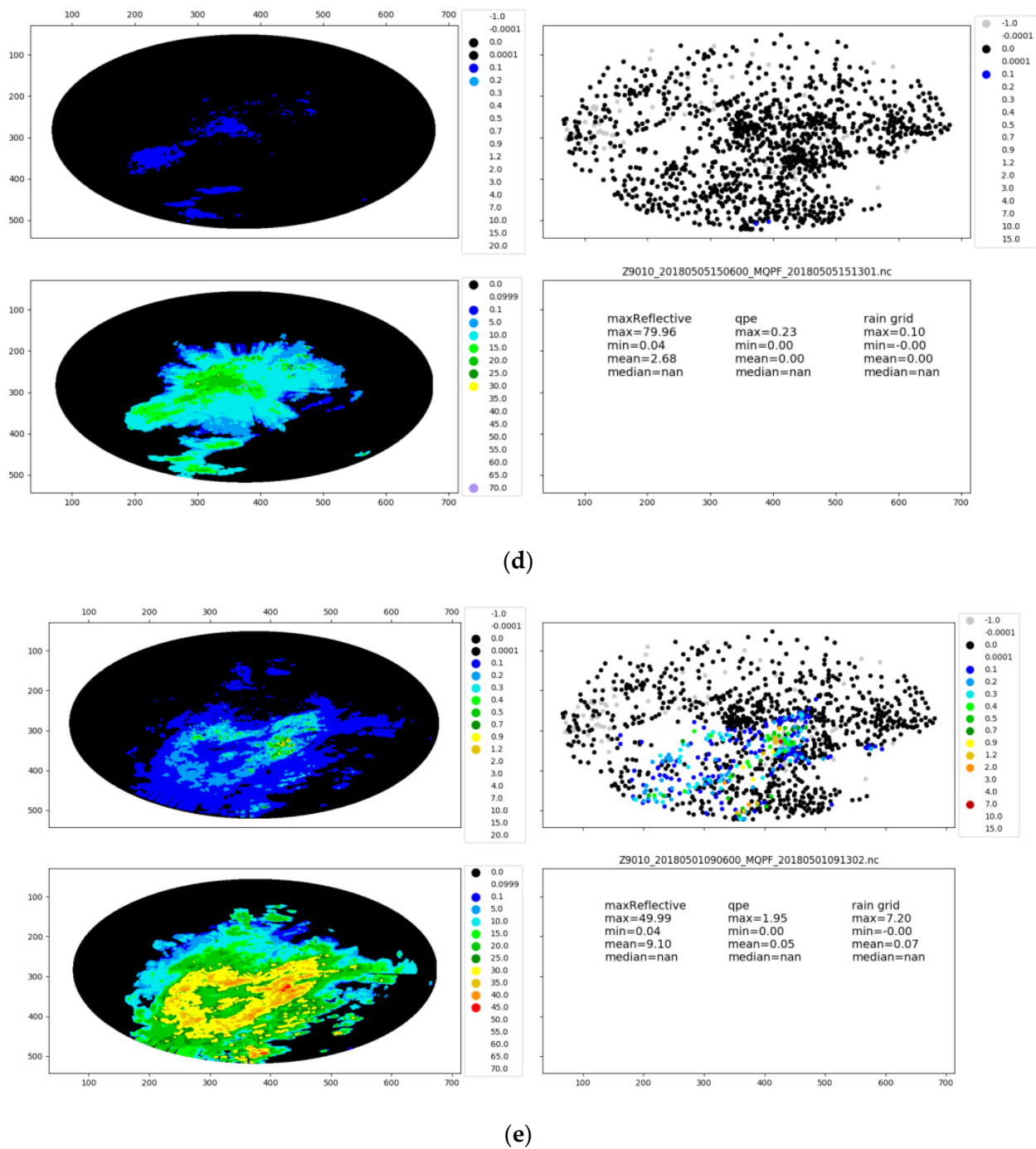


Figure 3. Examples of 5 echo types. The upper left subgraph shows the estimated value of MQPF. The lower left subgraph shows the combined reflectivity of radar echo. The upper right subgraph shows the observed precipitation of weather stations. The lower right subgraph on the right shows the statistical information. (a) Point nonprecipitation echo; (b) flake nonprecipitation echo; (c) clear sky nonprecipitation echo; (d) clear sky mixed flake nonprecipitation echo; (e) precipitation echo.

The specific steps of precipitation/nonprecipitation echo monomer recognition algorithm are as follows:

A. One month of Beijing radar 3D echo data are selected as the algorithm research dataset, and the data are manually labeled.

B. The radar echo area histogram and graded intensity ratio of each layer are extracted as the characteristics of radar echo data. The number of cell area lattices of each echo layer

in the three-dimensional echo is taken as the area for statistics to calculate the radar echo area histogram. In our study, the histogram group spacings are set as [1, 10, 20, 50, 100, 200, 250, 400, 1000, 2000, 5000, 10,000, 20,000, 50,000, 100,000, 200,000, 500,000, 10,000,000]. When calculating the graded intensity ratio, taking [0, 10, 20, 25, 40] as the graded intensity of the echo, the proportions of echo greater than or equal to this intensity value in the volume scanning area of the whole layer are calculated.

Feature dimension (N):

$$N = N_{\text{level}} \times (N_{\text{bin}} + N_{\text{ratio}}) \tag{1}$$

where N_{level} is the level of three-dimensional radar echo layer, N_{bin} is the number of groups of echo area histogram, and N_{ratio} is the number of intensity grades. In our study, $N_{\text{level}} = 21$, $N_{\text{bin}} = 17$, $N_{\text{ratio}} = 5$, so the feature dimension (N) = 462.

C. Sample data preprocessing: In order to avoid the division operation with zero denominator, the effective echo area zero values are uniformly changed to -1 . Then, the sample data are randomly divided into the training datasets and the testing datasets, in which the number of the training datasets accounts for 2/3 and the number of the testing datasets accounts for 1/3.

D. The SVM algorithm is used for multiclassifier training. The one-to-one method is used for the training of multiple classifiers. In our study, a total of $5 \times (5 - 1)/2 = 10$ SVM classifiers need to be designed for the five categories. During sample prediction, the category with the most votes confirmed by voting is the prediction category.

The model results are verified on the testing datasets. The results show that the trained multiclassifier can distinguish precipitation echo and different kinds of nonprecipitation echo, and the classification accuracy of the algorithm is 87.9% (Figure 4).

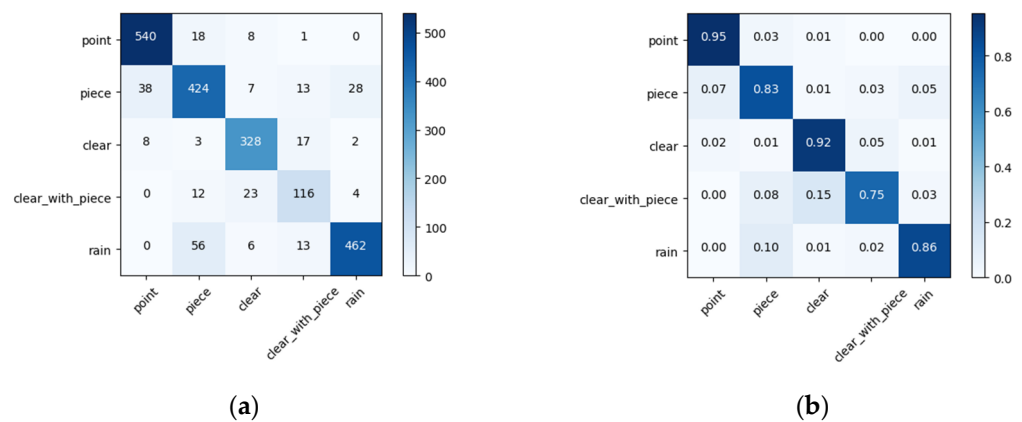


Figure 4. Confusion matrix of model validation results, with abscissa and ordinate representing the observations and predictions, respectively. Panels (a,b) represents the non-normalized and normalized confusion matrix, respectively.

Radar Monomer Recognition Technology Based on Region Segmentation

Based on the spatial adjacency of radar echo monomer, the radar monomer is recognized by using the region segmentation technology in image processing (Figure 5). The specific steps are as follows:

A. Based on experience, set four thresholds for echo value:

$T_1 = 10$ dBZ, represents the nonprecipitation echo threshold dominated by nonmeteorological echo;

$T_2 = 20$ dBZ, represents the echo threshold with coexistence of meteorological echo and nonmeteorological echo;

$T_3 = 30$ dBZ, represents the echo threshold which is mainly meteorological echo and is likely to produce precipitation;

$T_4 = 40$ dBZ, represents the meteorological echo threshold that will produce precipitation.

Corresponding to four intervals (0, 10], (10, 20], (20, 30], (30, 80), the echo data are mapped to the corresponding interval, and the threshold value is used to replace the original echo value. Other values greater than 30 dBZ are assigned 40 dBZ.

B. The echo edge and outlier echo are smoothed by the mean filtering.

C. The connected region is segmented by region labeling algorithm, and then the adjacency relationship of pixels is judged by an eight-connected domain algorithm [30].

D. Radar monomer data structure, including block information of echo and attribute information related to monomer area, are generated.

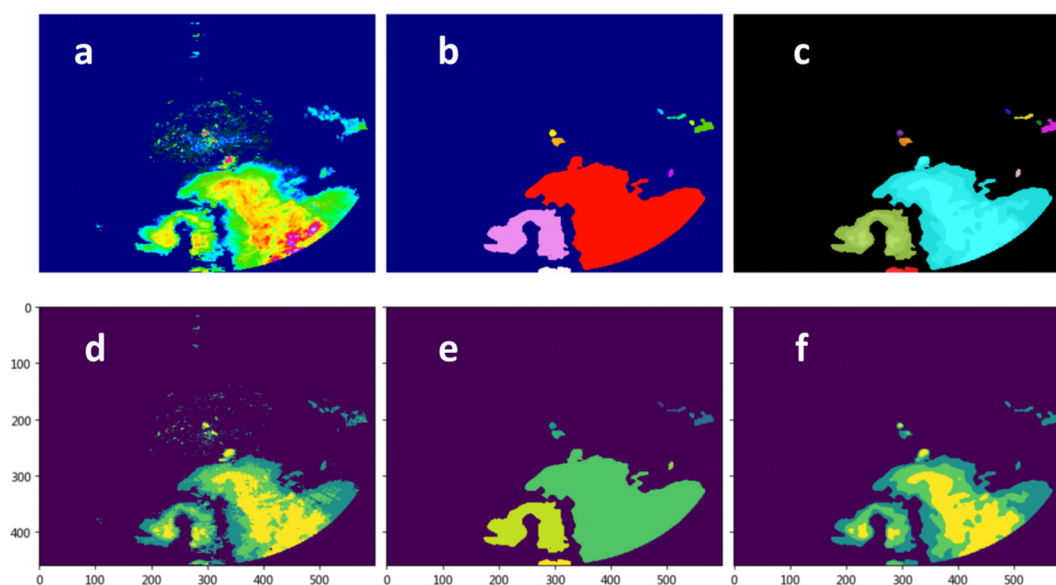


Figure 5. The results of radar monomer recognition based on image segmentation. (a) Original radar echo. (b) The result after monomer recognition. (c) The result after monomer segmentation. (d) The threshold segmentation result. (e) The monomer marking result. (f) The result after the mean filtering.

2.2.2. The Spatial Error Correction Technology Based on Linear Interpolation

The spatial error correction technology based on linear interpolation aims to calculate the precipitation estimation error on the weather stations according to the difference between MQPF and ground weather stations rainfall after obtaining the rainfall data of ground weather stations, and then generalizes the error to grid points through linear interpolation.

(1) Data preprocessing of ground weather stations

Main steps of the historical observation preprocessing:

- (A) Obtain the historical observation of minute level ground precipitation in the past 1 h through the rolling delay of 3 h through the data website service interface, and store the data every minute in a file.
- (B) By matching by station IDs, the minute precipitation within an hour is archived to a file. During this period, the data downloaded within hours are incomplete or the longitude and latitude information of the station cannot match.
- (C) According to the ground station number information obtained by the specified radar, the documents and contents are retrieved through time period, station number, and other information. Obtain an array with one row by station number and one column by minute.
- (D) Accumulate the data according to the station number to obtain the accumulated rainfall data in the time period corresponding to each station number.

Main steps of real-time data interface processing:

- (A) Start the scheduled task every 5 min to obtain the minute precipitation observation from the past 10 min to the past 5 min. Count the latest 5 min accumulated data and the latest accumulated data in the past 2 h, create the latest data table, respectively, and store the data in the table.
- (B) After that, clean up the data stored in the database for more than 3 h and back up the data. The background automatically calculates the radar ground station correspondence table every hour and stores it in the dictionary configuration file.
- (C) Through the front-end web interface, the precipitation accumulation information of the corresponding station is obtained according to the radar number and time, and the data are saved in CSV format.

(2) Spatial error correction based on linear interpolation

The main aim of spatial error correction is to generalize the station error to the grid. The spatial distribution of precipitation is uneven, so the error correction mainly depends on the distribution of ground stations. Considering the operation speed, linear interpolation is used to correct the spatial error. The main steps are as follows:

- (A) Based on the radar number and product time, the corresponding ground station observation is obtained through the historical observation text/real-time data web interface.
- (B) According to the longitude and latitude information of the ground station, the QPE on the corresponding grid point is obtained, and then the radar precipitation estimation error on the station is calculated.
- (C) The radar precipitation estimation error on the station is interpolated to the grid by linear interpolation algorithm to generate the radar precipitation estimation error of the grid field.
- (D) The grid radar precipitation estimation error is added to the radar precipitation estimation field, and finally the revised radar precipitation estimation field is obtained.

Figure 6 shows an effect diagram of spatial error correction technology based on linear interpolation.

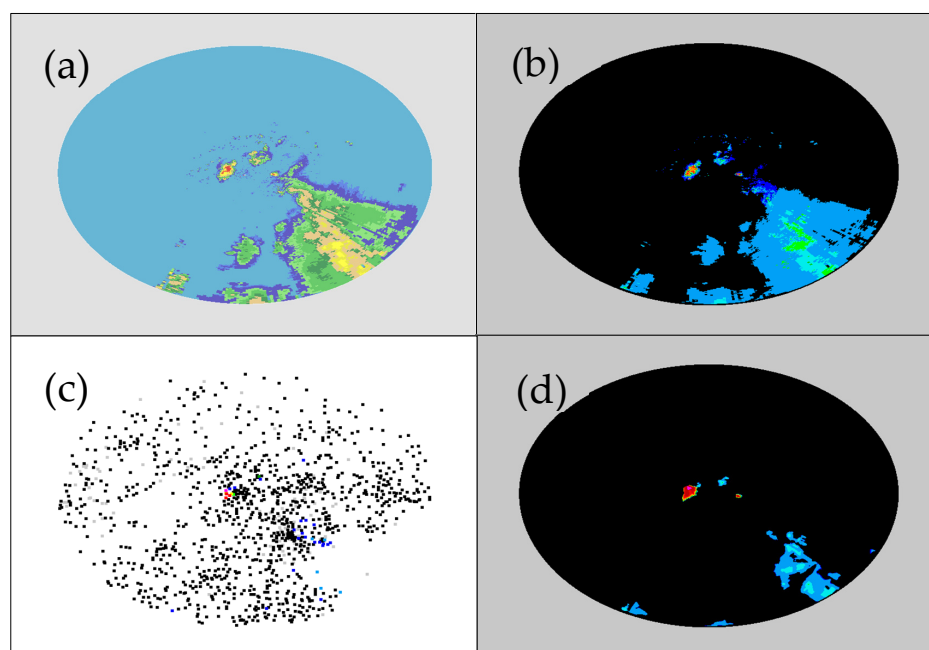


Figure 6. The correction effect display of the spatial error correction technology based on linear interpolation. (a) Radar echo live. (b) The uncorrected radar precipitation estimation field. (c) The 5 min actual precipitation at ground stations. (d) The revised radar precipitation estimation field.

2.2.3. The Temporal Error Correction Technology Based on Linear Interpolation

The temporal error correction technology based on linear regression mainly analyzes the precipitation change in the past two hours through linear regression method, determines the parameters of precipitation change trend, and is used to revise the precipitation forecast in the next two hours. The ground station data preprocessing refers to the contents in Section 2.2.2 (1) of this chapter and uses the same data processing method. The difference from the spatial error correction in Section 2.2.2 is that the temporal error correction accumulates the precipitation in the past 2 h and 5 min, while the spatial error correction accumulates the precipitation in the past 5 min. The main steps of temporal error correction include:

- (A) Based on the radar ID and product time, the data of the corresponding ground station in the past 2 h and 5 min can be obtained through the historical observation text/real-time data web interface.
- (B) The change slope S of the number of precipitation stations in the past 2 h, the change slope A of the mean precipitation of all stations in the past 2 h, and the change slope R of the mean precipitation of stations with rainfall in the past 2 h are calculated by linear regression. Among them, S reflects the change of precipitation area, A reflects the change of regional average precipitation efficiency, and R reflects the change of precipitation intensity of precipitation clouds (Figure 7). Then, the calculation formulas of rain intensity calculation variation coefficient m and n are

$$m = \begin{cases} 1.0 + A & S \leq 0 \\ 1.0 & \text{others} \end{cases} \quad (2)$$

$$n = \begin{cases} -R & S > 0 \text{ and } R \text{ exists} \\ -R \times 2 & S \leq 0 \text{ and } R \text{ exists} \\ 0.0 & R \text{ dose not exist} \end{cases} \quad (3)$$

$$m = \min(m, 1.01) \quad (4)$$

$$n = \max(n, 0) \quad (5)$$

$$n = \begin{cases} \max(n, -0.01) & n > -0.01 \text{ and } n < 0.01 \\ 0.0 & \text{others} \end{cases} \quad (6)$$

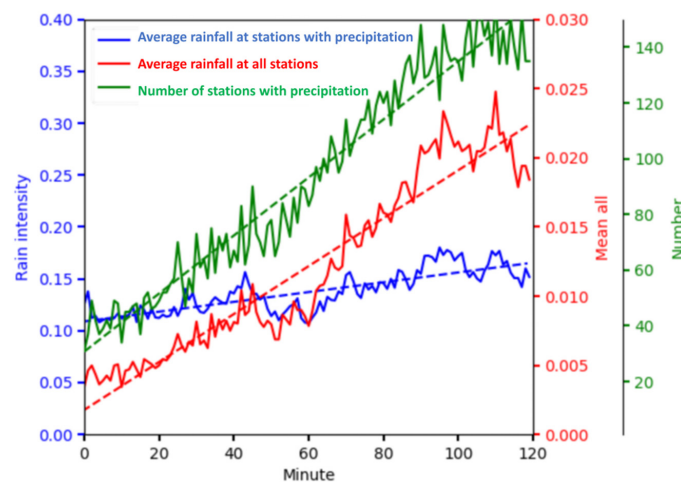


Figure 7. Time series of precipitation variables in the past two hours. The green line, red line, and blue line represent the number of precipitation stations in the past 2 h, the mean precipitation of all stations in the past 2 h, and the mean precipitation of stations with rainfall in the past 2 h, respectively.

- (C) According to the calculated regression coefficients m and n , the revised quantitative precipitation forecast (QPF) value is calculated.

$$QPF = m \times QPF + b \quad (7)$$

2.3. Model Evaluation

For model rainfall evaluation, using the forecast and observed, one set of yes/no for different intensity rainfall events are determined. The results could be placed into a 2×2 contingency table (Table 1). Then, the widely used statistical scores [31–33], that is, the threat score (TS), the false alarm ratio (FAR), and the missing ratio (MR) are used to evaluate the precipitation forecast accuracy. Their calculation method is as follows:

Table 1. Contingency table used to evaluate forecasts.

	Yes Observed	No Observed	The Total
Yes forecast	NA	NB	NA + NB
No forecast	NC	ND	NC + ND
The total	NA + NC	NB + ND	

The formula of TS in the specified time period is

$$TS = \frac{\sum NA}{\sum NA + \sum NB + \sum NC} \quad (8)$$

where NA, NB, and NC are the events per unit time, respectively, and $\sum NA$, $\sum NB$, and $\sum NC$ are the sums of NA, NB, and NC in the specified time period, respectively.

The value range of TS is 0–1, and the prediction effect is the best when the score is 1. TS mainly examines the matching degree between predicted events and actual events. The TS does not distinguish the source of prediction error, and because some hits may be random, the TS depends on the climate frequency of events (the TS will be lower for rare events).

The formula of FAR in the specified time period is

$$FAR = \frac{\sum NB}{\sum NA + \sum NB} \quad (9)$$

The value range of FAR is 0–1, and the prediction effect is the best when the score is 0. It measures how much of what is predicted to happen does not happen in real world.

The formula of MR in the specified time period is

$$MR = \frac{\sum NC}{\sum NA + \sum NC} \quad (10)$$

The value range of MR is 0–1, and the prediction effect is the best when the score is 0. The proportion of events measured in real life was not predicted.

3. Results

Taking the 2018 whole year as the testing period, 154 assessment stations in Beijing were selected as the testing stations, and the precipitation of 0.05 mm was regarded as the threshold between sunny and rainy. Our study calculated the performance indicators of Beijing single station products of MQPF and the performance indicators of Beijing single station observed minute precipitation, including the TS, FAR, and MR.

For the test of spatial error correction, the 5 min accumulation of ground actual precipitation was taken as the true value to test the radar QPE products of MQPF before and after our proposed correction. For the test of temporal error correction, the 30 min cumulative value of the ground actual precipitation was mainly taken as the true value to

test the 30 min cumulative values of radar QPF products before and after our proposed correction. For the timeliness test, we took the preparation of the front-end data of the revised algorithm as the start time and the generated result data of the algorithm operation as the end time, calculated the time spent by the algorithm operation at each time, and conducted statistical analysis.

3.1. Test of the Spatial and Temporal Error Correction Results

There are obvious differences in the number of precipitation samples between different months (Figure 8). From the sample size of different months, there were fewer precipitation samples from January to March and October to December, while there were relatively more samples in other months. Months with relatively few samples also had relatively low revised TS. For spatial error correction, except for January, February, and December, TS increased in other months. From the results before and after the spatial error correction, the annual FAR and MR changed from 0.7677 and 0.2602 to 0.0244 and 0.4015 (Figure 8). At the same time, the annual TS significantly improved, increasing to 0.5897 from 0.2147, an overall increase of 37.5%. This means that the method proposed in our study can significantly reduce the FAR, but it can also lead to an increase in the MR.

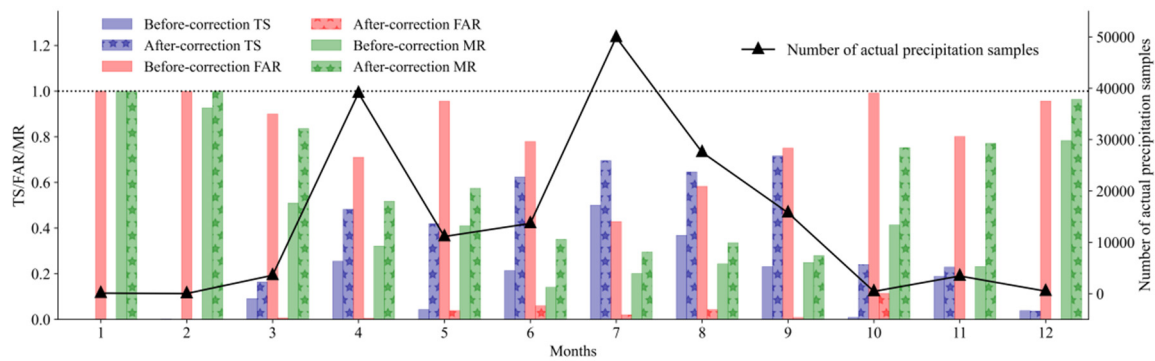


Figure 8. Test indices before and after the spatial error correction.

There was an obvious difference in the number of precipitation samples in the 30 min cumulative precipitation between different months, and the distribution was roughly the same as the 5 min cumulative precipitation corresponding to the radar QPE (Figure 9). Similar to the results of spatial error corrections, the corrected TS for months with relatively few samples was also relatively low. For time error correction, there was a significant increase for TS during April to October, while there was no increasing or a small increasing TS in the remaining months. Similar to the results of spatial error corrections, the method proposed in our study can significantly reduce the FAR, but it can also lead to an increase in the MR for the temporal error correction. The annual FAR and MR changed from 0.7212 and 0.3064 to 0.162 and 0.5222, and the TS increased from 0.2482 to 0.4374 an overall increase of 18.9%.

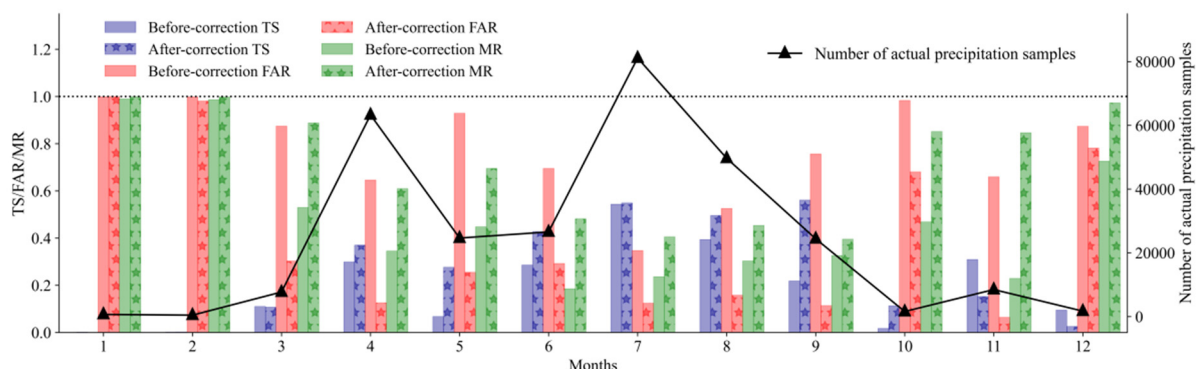


Figure 9. Test indices before and after the temporal error correction.

3.2. Test of Algorithm Timeliness

In order to effectively implement the rolling real-time update correction of the spatial error correction algorithm and the temporal error correction algorithm, it is necessary to ensure that the algorithm is completed before the arrival of the next radar base data (the interval between two radar volume scans is approximately 6 min). In the study, the algorithm timeliness was tested and verified through a server with CPU 24 cores and 64 GB of memory. The test results are shown in Table 2.

Table 2. Running time information of rolling real-time correction technology (unit: s).

Month	The Mean Running Time of Spatial Error Correction	The Longest Running Time of Spatial Error Correction	The Shortest Running Time of Spatial Error Correction	The Mean Running Time of Temporal Error Correction	The Longest Running Time of Temporal Error Correction	The Shortest Running Time of Temporal Error Correction
1	4.7	7.8	2.0	9.8	15.2	7.7
2	5.4	9.6	3.0	11.5	16.7	9.4
3	5.0	23.6	1.5	10.8	34.5	8.0
4	5.2	56.3	1.5	10.0	81.8	3.8
5	6.4	20.1	1.1	10.6	37.4	3.7
6	5.0	8.8	2.0	9.8	14.4	7.6
7	4.5	8.9	1.6	8.6	16.2	6.1
8	3.9	7.7	1.8	7.7	13.0	5.8
9	3.9	7.5	1.8	8.0	12.3	6.4
10	3.8	7.2	1.8	8.1	13.1	6.5
11	4.3	17.6	0.9	7.9	24.0	3.4
12	6.3	17.3	0.2	12.8	26.0	0.3

The mean running time to achieve correction of spatial and temporal error corrections ranged from 3.8 s in October to 6.4 s in May and 7.7 s in August to 11.5 s in February, respectively (Table 2). The longest time of spatial and temporal error corrections ranged from 7.2 s in October to 56.3 s in April and 12.3 s in September to 81.8 s in April, respectively. The shortest time of spatial and temporal error corrections ranged from 0.2 s in December to 3.0 s in February and 0.3 s in December to 9.4 s in February, respectively. From the above results, both temporal and spatial corrections take the longest time in April and the shortest time in December. This may be due to the relatively complex precipitation process starting from March and April, and the frequent correction, making it more time-consuming. However, in December, the rainfall is sparse, reducing the number of samples to be corrected, and, at the same time, shutting down some radars. Therefore, the revised model ran faster.

It is also possible for the same reason that the maximum value of each runtime indicator appears in the first half of the year (with the maxima spatial error correction mean running time appearing in May, the maxima spatial and temporal error correction longest running time appearing in April, and the maxima spatial error correction shortest running time, the temporal error correction mean, and shortest running time appearing in February), while the minimum value of the runtime indicator appears in the second half of the year (with the minima error correction mean and longest running time appearing in October, the minima spatial and temporal error correction shortest running time appearing in December, the minima temporal error correction mean running time appearing in August, and the minima temporal error correction longest running time appearing in September). Compared to the weather radar scanning every six minutes, the above time is sufficient to meet the requirements of real-time operation, and this method can be effectively applied in real-time operation. In terms of the update frequency of volume scan data, compared to precipitation estimation products with a long volume scan period (about 6 individual scan data in 1 h), radar precipitation estimation results with a high volume scan frequency (about 12 individual scan data in 1 h) are closer to those of rain gauges, with improved

accuracy [34]. Therefore, in view of its high timeliness, the method proposed in this study has strong universality.

4. Discussion

For spatial error correction, based on years of application experience and support vector machine algorithm models, we classified radar echoes into five categories: point nonprecipitation echo, flake nonprecipitation echo, clear sky nonprecipitation echo, clear sky mixed flake nonprecipitation echo, and precipitation echo. In the future, further identification will be carried out based on region segmentation technology. There are also other common methods of classifying radar echoes based on precipitation types in other studies, mainly dividing radar echoes into convective precipitation or layered precipitation echoes [35,36]. The month with more precipitation samples had a higher corrected TS, while the month with fewer had lower corrected TS. Li et al. [22] pointed out that the precipitation value of the original radar QPE product is too low, resulting in only a slight increase in precipitation through correction and fusion. It can be seen that a sufficient sample size and sufficient precipitation are the data basis for improving the correction effect.

The three-dimensional echo data used in this study had undergone preliminary quality control, but due to the performance of quality control algorithms, it was not possible to identify all nonmeteorological echoes and clear sky echoes. From the perspective of radar, although the application of polarization radar has not been widely studied in China, weather radar is gradually upgrading to this technology. Compared with traditional single polarization radar, dual-polarization radar has been proven to have better QPE performance [37–39]. We will continue to pay attention to the related technologies of dual-polarization radar in the future and attempt to transplant and apply these technologies. In addition, as another very advanced precipitation estimation technology, satellite precipitation estimation, supporting measurement of drizzle or fine raindrops, has been studied by many scholars [40–43]. Based on the fact that satellites can cover a wide range of observations, meet high-precision requirements, and their derived precipitation-related products also play an important role in the monitoring and analysis of rainstorm processes, it is also a very useful method to integrate satellite products into our research in future work.

5. Conclusions

Based on minute-level surface precipitation data, the rolling real-time correction technique for MQPF was proposed. Through the development of key technologies such as radar echo monomer extraction, spatial error correction based on linear interpolation, and temporal error correction based on linear regression, a technical process for minute precipitation product correction was established. After using this method for correction, the missed reporting rate of the 30 min cumulative precipitation forecast for the product can be significantly reduced, and the overall TS can be improved, which will have a positive impact on the quality improvement of short-term meteorological service products. From the perspective of running time, the method proposed in our study runs in an average of seconds, with a maximum running time of no more than 3 min, and can meet the real-time running requirements.

This study is currently only a preliminary study of the rolling real-time correction technology for weather radar minute precipitation forecast products. Future work will consider introducing other data and information such as satellite products to further complete the correction effect, and combine new artificial intelligence algorithms to improve the method performance. After further upgrades, this method is expected to be promoted and used on official weather websites or apps.

Author Contributions: Writing—original draft, J.D. and J.G.; writing—review and editing, J.D.; supervision, G.Z., F.Z. and J.Y.; data curation, S.W., B.X., J.G. and K.W.; methodology, J.G.; visualization, J.D. All authors have read and agreed to the published version of the manuscript.

Funding: This study is supported by the National Key Research and Development program of China (2020YFB1600103) and the National Natural Science Foundation of China (grants 41871020).

Data Availability Statement: No new data were created.

Conflicts of Interest: The authors declare no conflict of interest.

References

1. Xie, X.; Tian, Y.; Wei, G. Deduction of sudden rainstorm scenarios: Integrating decision makers' emotions, dynamic Bayesian network and DS evidence theory. *Nat. Hazards* **2022**, *116*, 2935–2955. [[CrossRef](#)]
2. Liu, Z.; Xu, J.; Liu, M.; Yin, Z.; Liu, X.; Yin, L.; Zheng, W. Remote sensing and geostatistics in urban water-resource monitoring: A review. *Mar. Freshw. Res.* **2023**. [[CrossRef](#)]
3. Tian, H.F.; Huang, N.; Niu, Z.; Qin, Y.C.; Pei, J.; Wang, J. Mapping Winter Crops in China with Multi-Source Satellite Imagery and Phenology-Based Algorithm. *Remote Sens.* **2019**, *11*, 820. [[CrossRef](#)]
4. Arno, G.; Hadi, P.; Suprayogi, S.; Herumurti, S. Daily quantitative precipitation estimates use weather radar reflectivity in South Sulawesi. *IOP Conf. Ser. Earth Environ. Sci.* **2018**, *256*, 012042. [[CrossRef](#)]
5. Marshall, J.S.; Palmer, W. The distribution of raindrops with size. *J. Meteor.* **1948**, *5*, 165–166. [[CrossRef](#)]
6. Gilewski, P.; Nawalany, M. Inter-Comparison of Rain-Gauge, Radar, and Satellite (IMERG GPM) Precipitation Estimates Performance for Rainfall-Runoff Modeling in a Mountainous Catchment in Poland. *Water* **2018**, *10*, 1665. [[CrossRef](#)]
7. Gualpa, M.; Orellana-Alvear, J.; Bendix, J. Tropical Andes Radar Precipitation Estimates Need High Temporal and Moderate Spatial Resolution. *Water* **2019**, *11*, 1038. [[CrossRef](#)]
8. Zhang, J.; Howard, K.W.; Langston, C.; Kaney, B.; Qi, Y.; Tang, L.; Grams, H.; Wang, Y.; Cocks, S.; Martinaitis, S.M.; et al. Multi-Radar Multi-Sensor (MRMS) Quantitative Precipitation Estimation: Initial Operating Capabilities. *Bull. Am. Meteorol. Soc.* **2016**, *97*, 621–638. [[CrossRef](#)]
9. Ware, E.C. Corrections to radar-estimated precipitation using observed rain gauge data. Master's Thesis, Cornell University, Ithaca, NY, USA, 2005; 96p.
10. Tong, Y.F.; Lai, S.T.; Tong, Y.F.; Lai, E. Applications of NWP and Nowcasting Techniques for the Warning of Rainstorms and Landslips. In Proceedings of the Tenth WMO Symposium on Education and Training, "Meteorological and Hydrological Education and Training for Disaster Prevention and Mitigation", Nanjing, China, 18–22 September 2008.
11. Ding, J.; Zhang, G.; Gao, J.; Wang, S.; Wang, K.; Xue, B.; Zhang, F.; Yang, J. Verification of the National Radar Minute Precipitation Method Applied in the Area precipitation Forecast—Taking Chaohu as an Example. *J. Anhui Agric. Sci.* **2021**, *49*, 221–225. (In Chinese) [[CrossRef](#)]
12. Wu, S.; Pan, T.; Cao, J.; He, D.; Xiao, Z. Barrier–corridor effect of longitudinal range–gorge terrain on monsoons in Southwest China. *Geogr. Res.* **2012**, *31*, 1393–1406. (In Chinese) [[CrossRef](#)]
13. Gu, J.; Shi, C.; Yang, P. Advances in research of the weather radar quantitative precipitation estimation. *Adv. Meteorol. Sci. Technol.* **2018**, *8*, 71–78. (In Chinese) [[CrossRef](#)]
14. Feng, L.; Zhou, T.; Wu, B.; Li, T.; Luo, J.-J. Projection of future precipitation change over China with a high-resolution global atmospheric model. *Adv. Atmospheric Sci.* **2011**, *28*, 464–476. [[CrossRef](#)]
15. Wong, M.C. From SWIRLS to RAPIDS: Nowcast applications development in Hong Kong. In Proceedings of the PWS Workshop on Warnings of Real-Time Hazards by Using Nowcasting Technology, Sydney, Australia, 9–13 October 2006.
16. Wong, W.K.; Yeung, L.H.; Wang, Y.C.; Chen, M. Towards the blending of NWP with nowcast—Operation experience in B08FDP. In Proceedings of the WMO Symposium on Nowcasting, Whistler, BC, Canada, 30 August–4 September 2009; Volume 30, p. 24.
17. Chu, Z.; Ma, Y.; Zhang, G.; Wang, Z.; Han, J.; Kou, L.; Li, N. Mitigating Spatial Discontinuity of Multi-Radar QPE Based on GPM/KuPR. *Hydrology* **2018**, *5*, 48. [[CrossRef](#)]
18. Andersen, C.B.; Wright, D.B.; Thorndahl, S. Sub-Hourly to Daily Rainfall Intensity-Duration-Frequency Estimation Using Stochastic Storm Transposition and Discontinuous Radar Data. *Water* **2022**, *14*, 4013. [[CrossRef](#)]
19. da Silva, E.J.R.; Alves, C.N.; Campos, P.C.D.O.; e Oliveira, R.A.A.C.; Marques, M.E.S.; Amorim, J.C.C.; Paz, I. Comparison of Rain Gauge Network and Weather Radar Data: Case Study in Angra dos Reis, Brazil. *Water* **2022**, *14*, 3944. [[CrossRef](#)]
20. Yoon, S.-S.; Lee, B. Effects of Using High-Density Rain Gauge Networks and Weather Radar Data on Urban Hydrological Analyses. *Water* **2017**, *9*, 931. [[CrossRef](#)]
21. Jing, G.; Luo, L.; Xiao, H.; Guo, J.; Cui, X. Application research of dual-polarization radar in quality control of automatic rain gauge. *Meteorol. Mon.* **2020**, *46*, 1189–1198. (In Chinese) [[CrossRef](#)]
22. Li, X.; Zhang, W.; Huang, S.; Deng, W.; Zhou, X. Analysis of fusion test results on hourly precipitation from meteorological and hydrological stations and radar. *Torrential Rain Disasters* **2020**, *39*, 276–284. (In Chinese) [[CrossRef](#)]
23. Li, M.; Qi, Y.; Zhang, Z.; Guan, X. Improving the Detection Performance of Extreme Precipitation Observations Using a Radar-Gauge Merging Algorithm. *Chin. J. Atmos. Sci.* **2022**, *46*, 1523–1542. (In Chinese) [[CrossRef](#)]
24. Kim, T.-J.; Kwon, H.-H.; Lima, C. A Bayesian partial pooling approach to mean field bias correction of weather radar rainfall estimates: Application to Osungsan weather radar in South Korea. *J. Hydrol.* **2018**, *565*, 14–26. [[CrossRef](#)]
25. Ozkaya, A.; Yilmaz, A.E. Analyzing radar rainfall estimate errors with three vector norms: Application to weather radar rainfall data in Muğla, Turkey. *Theor. Appl. Clim.* **2022**, *149*, 103–117. [[CrossRef](#)]

26. Men, B.; Wu, Z.; Liu, H.; Tian, W.; Zhao, Y. Spatio-temporal analysis of precipitation and temperature: A case study over the Beijing–Tianjin–Hebei Region, China. *Pure Appl. Geophys.* **2020**, *177*, 3527–3541. [[CrossRef](#)]
27. Ding, J.; Zhang, G.; Yang, J.; Wang, S.; Xue, B.; Du, X.; Tian, Y.; Wang, K.; Jiang, R.; Gao, J. Temporal and Spatial Characteristics of Meteorological Elements in the Vertical Direction at Airports and Hourly Airport Visibility Prediction by Artificial Intelligence Methods. *Sustainability* **2022**, *14*, 12213. [[CrossRef](#)]
28. Ding, J.; Zhang, G.; Wang, S.; Xue, B.; Yang, J.; Gao, J.; Wang, K.; Jiang, R.; Zhu, X. Forecast of Hourly Airport Visibility Based on Artificial Intelligence Methods. *Atmosphere* **2022**, *13*, 75. [[CrossRef](#)]
29. Cristianini, N.; Taylor, J.S. *An Introduction to Support Vector Machines and Other Kernel-Based Learning Methods*; United Kingdom at the University Press: Cambridge, UK, 2000.
30. Li, J.; Liu, J. Measurement for area based on connected regions arithmetic. *Sci. Technol. Eng.* **2008**, *8*, 2492–2494. (In Chinese)
31. Hsu, J.; Huang, W.-R.; Liu, P.-Y.; Li, X. Validation of chirps precipitation estimates over taiwan at multiple timescales. *Remote Sens.* **2021**, *13*, 254. [[CrossRef](#)]
32. Huang, W.-R.; Liu, P.-Y.; Chang, Y.-H.; Liu, C.-Y. Evaluation and Application of Satellite Precipitation Products in Studying the Summer Precipitation Variations over Taiwan. *Remote Sens.* **2020**, *12*, 347. [[CrossRef](#)]
33. Yu, Z.; Wu, M.; Min, J.; Yan, Y.; Lou, X. Impacts of WRF model domain size on meiyu rainfall forecasts over Zhejiang, China. *Asia-Pacific J. Atmos. Sci.* **2021**, *58*, 265–280. [[CrossRef](#)]
34. Chen, H.; Wang, Z.; Wang, H.; Sun, J.; Guo, J.; Wang, Z. Research on a New Quantitative Precipitation Estimation Method Based on CINRAD-SA Dual Polarization Radar. *Meteorol. Sci. Technol.* **2022**, *50*, 611–622. (In Chinese) [[CrossRef](#)]
35. Yang, Y.; Chen, X.; Qi, Y. Classification of convective/stratiform echoes in radar reflectivity observations using a fuzzy logic algorithm. *J. Geophys. Res. Atmos.* **2013**, *118*, 1896–1905. [[CrossRef](#)]
36. Bangsawan, L.; Jatmiko, R.H.; Nurjani, E. The comparison of z-r relation methods on convective and stratiform rain of quantitative precipitation estimation (QPE) in east java area. In Proceedings of the International Conference on Radioscience, Equatorial Atmospheric Science and Environment and Humanosphere Science, Online, 22–23 November 2022; Springer: Berlin/Heidelberg, Germany, 2022. [[CrossRef](#)]
37. Xia, Q.; Zhang, W.; Chen, H.; Lee, W.-C.; Han, L.; Ma, Y.; Liu, X. Quantification of Precipitation Using Polarimetric Radar Measurements during Several Typhoon Events in Southern China. *Remote Sens.* **2020**, *12*, 2058. [[CrossRef](#)]
38. Zhang, Y.; Liu, L.; Wen, H. Performance of a Radar Mosaic Quantitative Precipitation Estimation Algorithm Based on a New Data Quality Index for the Chinese Polarimetric Radars. *Remote Sens.* **2020**, *12*, 3557. [[CrossRef](#)]
39. Zhang, J.; Tang, L.; Cocks, S.; Zhang, P.; Ryzhkov, A.; Howard, K.; Langston, C.; Kaney, B. A dual-polarization radar synthetic qpe for operations. *J. Hydrometeorol.* **2020**, *21*, 2507–2521. [[CrossRef](#)]
40. Peinó, E.; Bech, J.; Udina, M. Performance Assessment of GPM IMERG Products at Different Time Resolutions, Climatic Areas and Topographic Conditions in Catalonia. *Remote Sens.* **2022**, *14*, 5085. [[CrossRef](#)]
41. Ren, J.; Xu, G.; Zhang, W.; Leng, L.; Xiao, Y.; Wan, R.; Wang, J. Evaluation and Improvement of FY-4A AGRI Quantitative Precipitation Estimation for Summer Precipitation over Complex Topography of Western China. *Remote Sens.* **2021**, *13*, 4366. [[CrossRef](#)]
42. Xu, J.; Ma, Z.; Tang, G.; Ji, Q.; Min, X.; Wan, W.; Shi, Z. Quantitative Evaluations and Error Source Analysis of Fengyun-2-Based and GPM-Based Precipitation Products over Mainland China in Summer, 2018. *Remote Sens.* **2019**, *11*, 2992. [[CrossRef](#)]
43. Shen, Y.; Hong, Z.; Pan, Y.; Yu, J.; Maguire, L. China’s 1 km Merged Gauge, Radar and Satellite Experimental Precipitation Dataset. *Remote Sens.* **2018**, *10*, 264. [[CrossRef](#)]

Disclaimer/Publisher’s Note: The statements, opinions and data contained in all publications are solely those of the individual author(s) and contributor(s) and not of MDPI and/or the editor(s). MDPI and/or the editor(s) disclaim responsibility for any injury to people or property resulting from any ideas, methods, instructions or products referred to in the content.